November 11, 2005 Version 2.1

Mid-Infrared Diagnostics of Nuclear and Extra-Nuclear Regions in Nearby Galaxies

D.A. Dale[1], J.D. Smith[2], L. Armus[3], B.A. Buckalew[3], G. Helou[3], D.J. Hollenbach[4], T.H. Jarrett[3], R.C. Kennicutt[2], J. Moustakas[2], H. Roussel[3], K. Sheth[3], et al.

ABSTRACT

The *Spitzer Infrared Nearby Galaxies Survey* dataset includes low- and high-resolution spectral cubes and broadband imaging in the infrared for over 160 nuclear and extranuclear regions within 75 nearby galaxies spanning a wide range of morphologies, metallicities, luminosities, and star formation activity levels. Here we present mid-infrared diagnostic diagrams for a large portion of the *SINGS* sample plus archival data from the *Infrared Space Observatory* and the *Spitzer Space Telescope*. Our work solidifies and extends to lower luminosities progress made with *ISO* spectroscopy on starbursting and ultraluminous infrared galaxies. Various combinations of aperture-matched extractions of line and continuum fluxes and PAH feature equivalent widths lead to a variety of mid-infrared diagnostics that effectively constrain the dominant power source of a particular region. Several useful results arise from these mid-infrared diagnostics, including: i) It is difficult to distinguish between pure Seyfert and pure LINER sources; ii) Both starbursting nuclei and extranuclear regions stand apart from nuclei that are powered by accretion-powered disks; iii) Compared to starbursting nuclei, extranuclear regions typically separate even further from accretion-powered nuclei, especially for low-metallicity environments; iv) Instead of the traditional mid-infrared approach to differentiating between AGN and star-forming sources that utilizes high excitation lines, we show that strong low excitation cooling lines of X-ray dominated regions can alternatively be used.

Subject headings: infrared: galaxies — infrared: ISM

[1]Department of Physics and Astronomy, University of Wyoming, Laramie, WY 82071; ddale@uwyo.edu

[2]Steward Observatory, University of Arizona, 933 North Cherry Avenue, Tucson, AZ 85721

[3]California Institute of Technology, MC 314-6, Pasadena, CA 91101

[4]NASA/Ames Research Center, MS 245-6, Moffett Field, CA 94035

1. Introduction

A traditional method for characterizing galaxy nuclear power sources uses ratios of optical emission lines such as [O II]3727Å, Hβ4861Å, [O III]5007Å, Hα6563Å, and [N II]6584Å (e.g. Baldwin, Phillips, & Terlevich 1981; Kewley et al. 2001; Kauffmann et al. 2003). A plot of [O III]/Hβ versus [N II]/Hα, for example, will typically separate Seyferts, LINERs, and starburst nuclei. Since nuclei are often heavily shrouded by dust, especially Luminous and Ultraluminous Infrared Galaxies (LIRGs and ULIRGs), an important limitation to galaxy optical diagnostics is the effect of extinction. The advent of sensitive mid-infrared line data from the *Infrared Space Observatory* enabled astronomers to peer more deeply into buried nuclear sources and approach their classification from a new perspective (Genzel et al. 1998; Laurent et al. 2000; Sturm et al. 2002; Peeters, Spoon, & Tielens 2004). Genzel and collaborators were the first to show that excitation-sensitive indices based on mid-infrared line ratios correlate with the strength of polycyclic aromatic hydrocarbon (PAH) emission features. AGN in particular show weak PAH emission (e.g. Weedman et al. 2005). Mid-infrared lines observed by *ISO* were also used to probe the physical characteristics and evolution of purely starbursting nuclei (Thornley et al. 2000; Verma et al. 2003) and Galactic H II regions (Vermeij & van der Hulst; Giveon et al. 2002).

The unprecedented sensitivity and angular resolution afforded by the *Spitzer Space Telescope* allow even more detailed studies of galaxy nuclei (e.g. Armus et al. 2004; Smith et al. 2004). SINGS takes full advantage of *Spitzer*'s capabilities by executing a comprehensive, multi-wavelength survey of 75 nearby galaxies spanning a wide range of morphologies, metallicities, luminosities, and star formation activity levels. The sensitivity of *Spitzer* coupled with the proximity of the SINGS sample allows dwarf galaxy systems fainter than $L_{\rm FIR} \sim 10^7\ L_\odot$ to be spectroscopically probed in the infrared for the first time. In addition, prior to *Spitzer* the only extragalactic H II regions that were detectable with infrared spectroscopy resided in the Local Group (e.g. Giveon et al. 2002; Vermeij et al. 2002). In contrast, SINGS provides infrared spectroscopic data for nearly 100 extragalactic H II regions, residing in systems as near as Local Group members to galaxies as far as ∼25 Mpc. The SINGS dataset thus samples a wider range of environments than previously explored with infrared spectroscopy. The goal of this study is to explore whether mid-infrared diagnostics developed for luminous/ultraluminous galaxies and bright Galactic H II regions can be extended to the nuclear and extra-nuclear regions within normal and infrared-faint galaxies.

2. The Sample

2.1. Galaxy Nuclei

The sample of nuclear targets analyzed in this study derive from the *SINGS* Third Data Release. These 50 nuclei come from a wide range of environments and galaxies: low-metallicity dwarfs; quiescent ellipticals; dusty grand design spirals; Seyferts, LINERs, and starbursting nuclei of normal galaxies; and systems within the Local and M 81 groups.

2.2. Extra-Nuclear Regions

The 26 extranuclear sources studied in this work also come from the *SINGS* Third Data Release. These targets stem from the original set of 39 optically-selected sources listed in Kennicutt et al. (2003). The optically-selected OB/H II regions cover a large range of metallicity (0.1-3 $Z_\odot$), extinction-corrected ionizing luminosity ($10^{49}-10^{52}$ photons s^{-1}), extinction ($A_V \lesssim 4$ mag), radiation field intensity (100-fold range), ionizing stellar temperature ($T_{\rm eff} = 35-55$ K), and local H_2/H I ratio (< 0.1 to > 10). Additional extranuclear targets for the SINGS project have since been identified, based on their infrared properties, but their observations necessarily came later than the observations of the optically-selected targets. Those "Second Look" data will be the focus of a future paper.

3. The Data

3.1. *Spitzer* Infrared Spectroscopy Observations and Data Processing

The full *SINGS* observing program and the data processing are described in Kennicutt et al. (2003), Smith et al. (2004), and Dale et al. (2005). Here we briefly summarize the spectral observations and data processing relevant to this paper. High-resolution spectroscopy was obtained in the Short-High (10-20 μm), Long-High (19-38 μm), and Short-Low (5-14 μm) modules. Nuclei were generally mapped with a 3×5 grid (Short-High and Long-High) and a 1×18 grid (Short-Low), utilizing half-slit width and half-slit length steps. Extra-nuclear targets were observed with a similar scheme but with a 1×9 Short-Low grid. For a subset of ten sources with extended circumnuclear star formation we obtained slightly larger (6×10) Short-High nuclear maps. Owing to the different angular sizes subtended by the instruments, the resulting maps are approximately $57'' \times 31''$ and $57'' \times 18''$ in Short-Low (nuclear and extra-nuclear, respectively), $45'' \times 33''$ in Long-High, and $23'' \times 15''$ in Short-High (the 10 expanded Short-High nuclear maps are $40'' \times 28''$). All integrations are 60 s per pointing, except the Short-Low nuclear maps are 14 s per pointing. The effective integrations are longer since each location was covered 2-4 times.

The individual data files for a given spectral map were assembled into spectral cubes using the software CUBISM described in Kennicutt et al. (2003). The cube input data were pre-processed using version S12.0 of the *Spitzer Science Center* pipeline. Various post-processing steps within CUBISM are described in Smith et al. (2004). Short-Low sky subtraction was enabled via the extended off-source wings of the Short-Low module. Several cross-checks on the flux calibration were made between Short-Low, Short-High, Long-Low, Long-High, MIPS, and IRAC data. The absolute flux calibration uncertainty for the spectral data is estimated to be 25%; the uncertainy in line flux ratios is XX%.

Though the Short-High, Long-High, and Short-Low cubes all span different solid angles, the same extraction apertures were used for all cubes: one-dimensional spectra were extracted from the three-dimensional data using $\sim 23'' \times 15''$ apertures. Furthermore, the extraction apertures are centered on the optically-derived coordinates listed in Kennicutt et al. (2003); in general, the apertures are centered on infrared-bright emission regions, but unfortunately in the cases of NGC 5408 and Tololo 89 the infrared peaks outside our $\sim 23'' \times 15''$ apertures. Emission line and PAH feature fluxes and equivalent widths are derived from continuum-subtracted Gaussian fits to the lines and first- or second-order fits to the continua.

3.2. Archival Spectroscopy

ISO-SWS and *Spitzer* IRS line fluxes are drawn from the literature for a wide variety of sources including Galactic, Magellanic Cloud, and Local Group H II regions (Vermeij et al. 2002; Giveon et al. 2002; Peeters et al. 2002), and starburst and active galaxies (Genzel et al. 1998; Sturm et al. 2002; Verma et al. 2003; Armus et al. 2004; Peeters, Spoon, & Tielens 2004; Weedman et al. 2005; Haas et al. 2005). Equivalent widths of the 6.2 μm PAH feature were extracted from archival *ISO*-PHOT and *Spitzer* IRS data, when available. The field-of-view of the *ISO*-PHOT aperture, $24'' \times 24''$, provides a decent match to the Short-High extraction apertures described in § 3.1.

3.3. *Spitzer* Broadband Imaging: 24 μm

Spitzer HighRes observations do not always detect the underlying hot dust continuum emission; SINGS IRS HighRes spectroscopy is designed to measure *line* fluxes and thus line equivalent width measures via HighRes are unreliable. On the other hand, the SINGS program includes extensive MIPS (Rieke et al. 2004) 24 μm broadband imaging of all galaxies. We use the 24 μm data to normalize the line fluxes in some of our diagnostic diagrams. Sky-subtracted MIPS 24 μm fluxes are extracted from aperture cutouts matched to the Short-High field-of-view (§ 3.1). See Kennicutt et al. (2003) and Dale et al. (2005) for further details of the *SINGS* broadband imaging.

3.4. Optical Spectroscopy Observations and Data Processing

Optical spectrophotometry has been obtained for the SINGS project at the Steward Observatory Bok 2.3 m and the CTIO 1.5 m telescopes (Moustakas & Kennicutt 2006). A suite of spectral drift scans were taken to spatially map the various regions covered with the IRS spectroscopy program (see Kennicutt et al. 2003 for more details). The optical spectroscopy has spectral resolution of $\sim$8Å and covers 3600-7000Å so that the primary nebular emission lines can be studied (e.g.

[O II]3727, Hβ4861, [O III]5007, Hα6563, [N II]6584).

This work utilizes optical spectral drift scans integrated over both the central $2''.5\times2''.5$ and $20''\times20''$ regions, the latter of which approximately matches the circumnuclear regions over which the infrared line and PAH feature fluxes are extracted (see § 3.1).

4. Results

4.1. High-Resolution Infrared Spectroscopy: Emission Lines

Several forbidden lines are quite prominent in many of the SINGS nuclear and extra-nuclear high resolution spectra ([Ne II]12.81 μm, [Ne III]15.56 μm, [S III]18.71 μm, [S III]33.48 μm, [Si II]34.82 μm) along with a few other higher ionization lines that are occasionally observed ([S IV]10.51 μm, [Ne V]14.32 μm, [O IV]25.89 μm; Figure 1). All these lines except [Si II]34.82 μm are nebular lines from ionized gas; [Si II]34.82 μm comes from a wider variety of regions, including both ionized gas and warm atomic gas such as photo-dissociation regions and X-ray dominated regions. A series of interstellar molecular hydrogen lines are also detected in the *SINGS* spectra; these are explored in a separate paper (Roussel et al. 2006, in preparation). The line fluxes are listed in Table 2.

4.2. Low-Resolution Infrared Spectroscopy: The 6.2 μm PAH Feature

The strength of a PAH feature depends on a complex combination of several parameters of the interstellar medium, some of which are interlinked: metallicity, dust column density, the distribution of sizes and ionization states in the dust grain population, and the intensity and hardness of the interstellar radiation field (e.g. Cesarsky et al. 1996; Thuan et al. 1999; Sturm et al. 2000; Li & Draine 2001; Draine & Li 2001; Galliano et al. 2005; Engelbracht et al. 2005). Due to this sensitivity to the charateristics of the interstellar medium, PAH features in the mid-infrared have been used to characterize the physical state of a system. Previous efforts have utilized the 6.2 μm feature (Laurent et al. 2000; Peeters, Spoon, & Tielens 2004), the 7.7 μm feature (Genzel et al. 1998), or a combination of several PAH features (e.g. Verstraete et al. 2001; Tran et al. 2001; Peeters et al. 2002; Förster Schreiber et al. 2004; Armus et al. 2004; Peeters et al. 2004; Madden et al. 2005). For this work we adopt the sensible approach of Weedman et al. (2005) and concentrate on diagnostics that utilize the 6.2 μm feature. The 6.2 μm feature is perhaps the one strong infrared signature of PAHs for which the blue- and red-sides of the continuum are easy to define, there is no blending with an emission line or absorption trough, and is not near the wavelength edges of an IRS low resolution module (Houck et al. 2004). The equivalent widths of the 6.2 μm feature are listed in Table 2.

4.3. Optical Classifications of Nuclei

Not all of the SINGS galaxies have an optical nuclear classification in the literature (e.g. Seyfert, LINER, starburst, etc). Moreover, online databases such as NED[1] provide a heterogeneous source for such classifications. Thus we turn to our own optical spectroscopy. Figure 2 displays a traditional "BPT" diagram (Baldwin, Phillips, & Terlevich 1981) using optical spectroscopy and $2\farcs5\times2\farcs5$ apertures for SINGS galaxy nuclei. The dotted lines delineate typical starburst/AGN/LINER boundaries: [O III]5007/Hβ $\sim$ 5 and [N II]6583/Hα $\sim$ 0.6 (e.g. Armus, Heckman, & Miley 1989). The long-dashed and short-dashed curves respectively trace the empirical starburst/AGN boundaries of Kewley et al. (2001) and Kauffmann et al. (2003) who use hundreds to thousands of galaxies to define their curves. Filled circles in Figure 2 mark galaxies for which NED does not indicate an active nucleus (LINER or Seyfert); data points without filled circles in this diagram represent galaxies with AGN classifications on NED. It is evident that the classification information available from NED is insufficient for a handful of SINGS nuclei. NED does not indicate that the nuclei of NGC 1291, NGC 1512, NGC 3198, and NGC 3621 are dominated by AGN, whereas our spectroscopic data place them squarely in such a category.[2] For the purposes of the remainder of this study we consider these sources, along with all other sources with [N II]6583/Hα $>$ 0.6, to have AGN.

Using the Hα/Hβ ratio extracted from our optical spectra, the SINGS nuclei show modest attenuations (for a screen model), $A_V \sim 1.3$ mag with a dispersion of 1.0 mag. These values are the same whether we analyze the data from $2\farcs5\times2\farcs5$ or $20''\times20''$ aperture extractions centered on the nuclei. In short, no sources appear to be heavily buried in the optical so presumably none of the classifications are skewed by large amounts of dust. In addition, the SINGS sample shows a clean separation between nuclei dominated by AGN and nuclei dominated by star formation. There may be few if any transition objects that are difficult to interpret. In the next section we turn to the mid-infrared where we will perhaps more convincingly be able to determine whether the optical classifications are appropriate.

4.4. Infrared Diagnostics of Nuclei and Extra-Nuclear Regions

4.4.1. Emission Line Ratios and PAH Strength

The excitation potential of [O IV] is 54.9 eV; photons at least this energetic are required to remove an electron from doubly-ionized Oxygen. On the other hand, ionizing neutral Neon "only" requires 21.6 eV. Compared to 21.6 eV photons, 54.9 eV photons are far more likely to stem from

[1]NASA/IPAC Extragalactic Database

[2]Our optical line ratios also indicate that NGC 0584, NGC 1377, NGC 1404, and NGC 3938 also harbor AGN, but at a signal-to-noise less than three.

accretion-powered disks than star formation (e.g. OB stars), and thus the ratio of [O IV]25.89 μm and [Ne II]12.81 μm depends on the type of source dominating the energetics of the interstellar medium. Furthermore, studies show that PAH features are quite prominent throughout much of the interstellar medium save for regions characterized by exceptionally hard radiation fields such as arise in AGN (Cesarsky et al. 1996; Sturm et al. 2000). A mid-infrared diagnostic diagram first put forth by Genzel et al. (1998), and later explored by Peeters, Spoon, & Tielens (2004), plots the emission line ratio [O IV]25.89 μm/[Ne II]12.81 μm versus the strength of a mid-infrared PAH feature. In such plots AGN sources show enhanced [O IV]25.89 μm emission and comparatively weak PAH feature strength. However, those two studies focussed on AGN-dominated and starburst nuclei. The upper panel of Figure 3 uses the 6.2 μm PAH feature and the emission line ratio [O IV]25.89 μm/[Ne II]12.81 μm in a similar mid-infrared diagnostic diagram, but one that incorporates normal nuclei and H II regions. As expected, normal nuclei and H II regions extend the previously-observed trend: lower-luminosity star-forming nuclei and H II regions exhibit comparatively large 6.2 μm equivalent widths and relatively low ratios of [O IV]25.89 μm/[Ne II]12.81 μm, indicating strong contributions from [Ne II]12.81 μm cooling of H II regions and their PAH-rich photo-dissociation region surroundings, and negligible emission from accretion-powered disks.

High excitation lines like [O IV]25.89 μm are somewhat difficult to detect in many SINGS sources. An alternative diagnostic diagram is provided in the lower panel of Figure 3 involving the more easily detectable [Si II] 34.82 μm line. Since [Si II] has an excitation potential of 8.15 eV, the ratio of excitation potentials in the upper panel of Figure 3 is nearly the inverse of that in the lower panel, 2.55 versus 2.65^{-1}; one might arguably expect that the trend in the lower panel would be a mirror image of the trend in the upper panel, with relatively small values of [Si II]34.82 μm/[Ne II]12.81 μm for AGN-type sources compared to star-forming regions. Why, in fact, are similar trends seen in the two panels? The answer may lie in the physics of X-ray dominated regions. As pointed out by Maloney, Hollenbach, & Tielens (1996), the [Si II]34.82 μm line is a strong coolant of X-ray irradiated gas: "For hard-spectrum sources ... the emission from ... X-ray dominated regions completely dominates over emission from the negligibly small H II region that will also surround the source" and the "large column densities that can be traversed by hard X-ray photons result in large emitting volumes for the X-ray dominated regions, and the conversion of X-ray luminosity to infrared continuum and line emission can be quite efficient." Maloney, Hollenbach, & Tielens (1996) predict that [Si II]34.82 μm, [O I]63 μm, [C II]158 μm, and [C I]609 μm are the top four cooling lines within X-ray dominated regions, with 1-10% of the 1-100 keV luminosity reradiated as [Si II]34.82 μm for an extremely large range of physical conditions.

An argument based on interstellar density provides another possibility for the low [Si II]34.82 μm/[Ne II]12.81 μ ratio in AGN. Kaufman et al. (2006) show that the ratio [Si II](PDR)/[Si II](H II) increases with increasing density. In fact, for low density H II regions most of the [Si II] comes from the H II region and not the surrounding photo-dissociation region. Moreover, Meijerink & Spaans (2005) show that the ratio [Si II](XDR)/[Si II](PDR) also increases with increasing density. AGN may have their emitting gas at higher densities than typically found in starbursts and normal galaxies, leading to an increased [Si II]34.82 μm/[Ne II]12.81 μm ratio. In other words, if the [Si II] comes mostly from X-ray dominated regions, then the low [Si II]34.82 μm/[Ne II]12.81 μm for AGN sources is due to strong [Si II] cooling. If most of the [Si II] emission comes from photo-dissociation regions, then the low [Si II]34.82 μm/[Ne II]12.81 μm for AGN sources is due to enhanced [Si II] emission in dense photo-dissociation regions.

The dotted lines in Figure 3 represent a variable mix of an AGN nucleus and a "pure" star-forming H II region. The 100% AGN anchor for these mixing models have values of EW(PAH 6.2 μm)= 0.01 μm, [O IV]25.89 μm/[Ne II]12.81 μm=0.5, and [Si II]34.82 μm/[Ne II]12.81 μm=2, whereas the 100% star formation anchor has EW(PAH 6.2 μm)= 0.6 μm, [O IV]25.89 μm/[Ne II]12.81 μm=0.02, and [Si II]34.82 μm/[Ne II]12.81 μm=0.5. The dashed line in the upper panel of Figure 3 shows the approximate mixing model of Genzel et al. (1998), obtained after empirically deriving a relation between their 7.7 μm PAH 'strength' (line-to-continuum ratio) and the 6.2 μm PAH equivalent width. Many of the high excitation data presented in Genzel et al. (1998) were upper limits, so it makes sense that their original curve lies above our curve.

Finally, it should be noted that relatively strong low excitation line emission (e.g. [O I]6300Å and [O I]63 μm) has previously been observed emanating from the large "partially-ionized regions" surrounding AGN (Armus, Heckman, & Miley 1989; Veilleux 1991; Osterbrock 1993; Dale et al. 2004). Hence, strong low excitation line emission from AGN is not a new concept. Nonetheless, we present a new technique for distinguishing between AGN sources and star-forming regions, one that relies on an easily-detectable, prominant cooling line of a low-excitation species associated with X-ray dominated regions, the dense interstellar material illuminated by power-law radiation fields.

4.4.2. Excitation Line Ratios

Figure 4 plots a ratio of double- to single-ionized Neon as a function of a ratio of triple- to double-ionized Sulfur. Many of the data points in this plot are for Galactic H II regions (Vermeij et al. 2002; Giveon et al. 2002; Peeters et al. 2002; see § 3.2). Clearly the Neon excitation ratio tracks the Sulfur excitation ratio. To first order, there does not appear to be any sequence in the distribution according to source classification (Seyfert, starburst, H II, etc). However, the low-metallicity H II regions from the Magellanic Clouds are preferentially in the upper righthand corner of the diagram. Presumably the diminished line blanketing for low-metallicity sources results in a harder radiation field and thus higher excitation ratios. In addition, AGN sources show somewhat lower [Ne III]15.6 μm/[Ne II]12.81 μm ratios, and the locus of the AGN detections lie at slightly higher values of [S IV]10.51 μm/[S III]18.71 μm. The dotted and solid curves show linear fits to the AGN and star-forming sources, respectively.

4.4.3. Excitation and Metallicity

If the Neon excitation ratio is plotted as a function of [S III]33.48 μm/[Si II]34.82 μm (Figure 5), a more obvious separation of the star-forming and AGN-powered data points is observed. Not only do the low-metallicity Magellanic Cloud regions exhibit a higher ratio in the Neon excitation ratio, nearly all of the "pure star-forming" nuclei and extra-nuclear regions show relatively elevated ratios in [S III]33.48 μm/[Si II]34.82 μm. This result can be understood in the context of the cooling line physics introduced above. The [Si II]34.82 μm line is a significant coolant of X-ray dominated regions (Hollenbach & Tielens 1999), whereas the [S III]33.48 μm line is a strong marker of H II regions. In other words, extra-nuclear regions and star-forming nuclei will show strong signatures of the Strömgren sphere coolant [S III]33.48 μm, while AGN and their associated X-ray dominated regions will exhibit relatively strong [Si II]34.82 μm emission. Note in addition that many of the filled squares representing starbursting/star-forming nuclei are located between the H II regions and the AGN. Since the central regions of galaxies typically are more abundant in heavy metals (Pilyugin & Ferrini 1998), and as explained above a lower metallicity can lead to harsher radiation fields and thus enhanced high-excitation-to-low-excitation line ratios, it is possible that this AGN$\rightarrow$H II nucleus$\rightarrow$H II region sequencing along the [S III]33.48 μm/[Si II]34.82 μm axis is due to metallicity. Alternatively, perhaps some of these star-forming nuclei have contributions from undetected weak AGN and thus are not "pure" star-forming nuclei.

4.4.4. Density Diagnostics

The average line ratio of [S III]18.71 μm-to-[S III]33.48 μm for the SINGS sample is 0.82 with a 1σ dispersion of 0.27. This implies an interstellar electron density of $n_{\rm e} \sim 400^{+240}_{-290}$ cm^{-3} for the central regions of these galaxies (calculated using electron collision strengths from Tayal & Gupta 1999). A visual way to explore this line ratio is portrayed in Figure 6, where the set of dashed lines repesent different interstellar electron densities. The correlation in Figure 6 extends over two orders of magnitude in the line-to-continuum ratios and encompasses both AGN-dominated and star-formation-dominated sources; a non-parametric ranking analysis indicates a global correlation at the 7σ level. Linear fits to the two separate populations emphasize that, though the slopes in the trends for the two populations are similar, the nuclei with obvious AGN activity (dotted line) appear separately from the starbursting nuclei and the H II regions (solid line). Star-forming sources show more pronounced [S III]33.48 μm emission compared to AGN, consistent with the notion that [S III]33.48 μm is an important coolant of H II regions. Alternatively, we are seeing the effects of continuum dilution in the line-to-continuum ratio for AGN, sources for which hot dust emission is pronounced in the mid-infrared and thus the line-to-continuum ratios are suppressed (e.g. Laurent et al. 2000; Dale et al. 2001; Xu et al. 2001; Siebenmorgen et al. 2004). Finally, similar to what is seen in Figures 3 and 5, but perhaps not as prominently, the data in Figure 6 suggest that the H II regions (open squares) occupy a different portion of phase space than star-forming nuclei (filled squares). H II regions have higher line-to-continuum ratios than star-forming nuclei, which in turn have higher ratios than AGN.

5. Summary

We have presented mid-infrared diagnostic diagrams for a large portion of the *SINGS* sample plus archival *ISO* and *Spitzer* data. There are no SINGS sources sufficiently buried such that optical and infrared diagnostics provide obviously discrepant classifications of the energy source. This is not surprising, however, since our nuclei exhibit modest extinctions, $A_V \sim 1.3$ mag, and normal star-forming galaxy nuclei in general show $0 \lesssim A_V \lesssim 3$ mag (Ho, Filippenko, & Sargent 1997. The power of the "Genzel diagram" (Genzel et al. 1998; Peeters, Spoon, & Tielens 2004) for distinguishing between AGN and star-forming sources is that mid-infrared lines are much less affected by extinction than their optical counterparts in a traditional diagnostic diagram (Baldwin, Phillips, & Terlevich 1981). Our work solidifies and extends to lower luminosities previous *ISO*-based mid-infrared work to lower luminosity normal galaxy nuclei and H II regions using the *Spitzer Space Telescope*. A variety of mid-infrared diagnostics can effectively constrain the dominant power source of a particular region. Though it is difficult to distinguish between pure Seyfert and pure LINER sources, both starbursting nuclei and extranuclear regions stand apart from nuclei that are powered by accretion-powered disks. Moreover, compared to starbursting nuclei, extranuclear regions typically separate even further from accretion-powered nuclei, especially for low-metallicity environments. Finally, instead of the traditional mid-infrared approach to differentiating between AGN and star-forming sources that utilizes high excitation lines, we show that prominent low excitation cooling lines of X-ray dominated regions can alternatively be used in place of the relatively weak high excitation lines.

Mike Brotherton provided helpful comments. Support for this work, part of the *Spitzer Space Telescope* Legacy Science Program, was provided by NASA through Contract Number 1224769 issued by the Jet Propulsion Laboratory, California Institute of Technology under NASA contract 1407. This research has made use of the NASA/IPAC Extragalactic Database which is operated by JPL/Caltech, under contract with NASA. This publication makes use of data products from the Two Micron All Sky Survey, which is a joint project of the University of Massachusetts and the Infrared Processing and Analysis Center/California Institute of Technology, funded by the National Aeronautics and Space Administration and the National Science Foundation.

REFERENCES

Armus, L., Heckman, T.M., & Miley, G.K. 1989, ApJ, 347, 727

Armus, L. et al. 2004, ApJS, 154, L178

Baldwin, J.A., Phillips, M.M., & Terlevich, R. 1981, PASP, 93, 5

Calzetti, D. et al. 2005, ApJ, in press

Carranza, G., Crillon, R., Monnet, G. 1969 A&A, 1, 479

Cesarsky, D., Lequeux, J., Abergel, A., Perault, M., Palazzi, E., Madden, S., & Tran, D. 1996, A&A, 315, L309

Dale, D.A., Helou, G., Contursi, A., Silbermann, N.A., & Kolhatkar, S. 2001, ApJ, 549, 215

Dale, D.A., Helou, G., Brauher, J.R., Cutri, R.M., Malhotra, S., & Beichman, C.A. 2004, ApJ, 604, 565

Dale, D.A. et al. 2005, ApJ, in press

Draine, B.T. & Li, A. 2001, ApJ, 551, 807

Förster Schrieber, N.M., Roussel, H., Sauvage, M., & Charmandaris, V. 2004, A&A, 419, 501

Galliano, F., Madden, S.C., Jones, A.P., Wilson, C.D., & Bernard, J.-P. 2005, A&A, 434, 867

Genzel, R. et al. 1998, ApJ, 498, 579

Giveon, U., Sternberg, A., Lutz, D., Feuchtgruber, H., & Pauldrach, A.W.A. 2002, ApJ, 566, 880

Haas, M., Siebenmorgen, R., Schulz, B., Krügel, E., & Chini, R. 2005, A&A, in press

Ho, L., Filippenko, A.V., & Sargent, W.L. 1997, ApJ, 487, 579

Hodge, P.W. 1966, *An Atlas and Catalog of H II Regions in Galaxies* (Seattle: Astronomy Department, University of Washington)

Hollenbach, D. & Tielens, A.G.G.M. 1999, Rev. Mod. Phys., 71, 173

Houck, J.R. et al. 2004, ApJS, 154, L18

Kauffmann, G. et al. 2003, MNRAS, 346, 1055

Kaufman, M. et al. 2006, in preparation

Kennicutt, R.C. et al. 2003, PASP, 115, 928

Kewley, L.J., Dopita, M.A., Sutherland, R.S., Heisler, C.A., Trevena, J. 2001, ApJ, 556, 121

Laurent, O., Mirabel, I.F., Charmandaris, V., Gallais, P., Madden, S.C., Sauvage, M., Vigroux, L., & Cesarsky, C. 2000, A&A, 359, 887

Li, A. & Draine, B.T. 2001, ApJ, 554, 778

Madden, S.C., Galliano, F., Jones, A.P., & Sauvage, M. 2005, A&A, submitted

Maloney, P.R., Hollenbach, D.J., & Tielens, A.G.G.M. 1996, ApJ, 466, 561

Meijerink, R. & Spaans, M. 2005, A&A, 436, 397

Moustakas, J. & Kennicutt, R.C. 2006, ApJ, submitted

Osterbrock, D.E. 1993, ApJ, 404, 551

Peeters, E. et al. 2002, A&A, 381, 571

Peeters, E., Spoon, H.W.W., & Tielens, A.G.G.M. 2004, ApJ, 613, 986

Peeters, E., Mattioda, A.L., Hudgins, D.M., & Allamandola, L.J. 2004, ApJ, 617, L

Pilyugin, L.S. & Ferrini, F. 1998, A&A, 336, 103

Rieke, G.H. et al. 2004, ApJS, 154, 25

Siebenmorgen, R., Freudling, W., Krügel, E., & Haas, M., 2004, A&A, 421, 129

Smith, J.D.T. et al. 2004, ApJS, 154, L199

Sturm, E., Lutz, D., Tran, D., Feuchtgruber, H., Genzel, R., Kunze, D., Moorwood, A.F.M., & Thornley, M.D. 2000, A&A, 358, 481

Sturm, E., Lutz, D., Verma, A., Netzer, H., Sternberg, A., Moorwood, A.F.M., Oliva, E., & Genzel, R. 2002, A&A, 393, 821

Tayal, S.S., & Gupta, G.P. 1999, ApJS, 526, 544

Thornley, M.D., Förster Schreiber, N.M., Lutz, D., Genzel, R., Spoon, H.W.W., Kunze, D., & Sternberg, A. 2000, ApJ, 539, 641

Thuan, T.X., Sauvage, M., & Madden, S. 1999, ApJ, 516, 783

Veilleux, S. 1991, ApJ, 369, 331

Verma, A., Lutz, D., Sturm, E., Sternberg, A., Genzel, R., & Vacca, W. 2003, A&A, 403, 829

Vermeij, R. & van der Hulst, J.M. 2002, A&A, 391, 1081

Vermeij, R., Damour, F., van der Hulst, J.M., & Baluteau, J.-P. 2002, A&A, 390, 649

Verstraete, L., Pech, C., Moutou, C., Sellgren, K., Wright, C.M., Giard, M., Léger, A., Timmerman, R., & Drapatz, S. 2001, A&A, 372, 981

Weedman, D.W., Hao, L., Higdon, S.J.U., Devost, D., Wu, Y., Charmandaris, V., Brandl, B., Bass, E., & Houck, J.R. 2005, ApJ, 633, 706

Xu, C., Lonsdale, C.J., Shupe, D.L., O'Linger, J., & Masci, F. 2001, ApJ, 562, 179

Table 1. Nuclear Emission Line Fluxes and 6.2 μm PAH Feature Equivalent Widths [a]

Species Wavelength Excitation (eV)	PAH 6.2μm	[SIV] 10.51μm 34.8	[NeII] 12.81μm 21.6	[NeIII] 15.56μm 41.0	[SIII] 18.71μm 23.3	[OIV] 25.89μm 54.9	[SIII] 33.48μm 23.3	[SiII] 34.82μm 8.2
NGC 0337	0.63±0.05	···	30.3±1.2	14.7±0.8	26.5±1.3	···	38.0±0.7	38.4±1.1
NGC 0584								
NGC 0628								
NGC 1097								
NGC 1266								
NGC 1377								
NGC 1566								
NGC 1404								
NGC 1705								
Holmberg II								
DDO 053								
NGC 2798	0.52±0.02	8.75±2.3	350 ±3	62.1±0.9	165 ±2	17.1±3.4	152 ±5	183 ±5
NGC 2841								
NGC 2915								
NGC 2976								
NGC 3049								
Holmberg IX								
NGC 3190								
NGC 3184								
NGC 3198								
IC 2574								
NGC 3265								
Markarian 33								
NGC 3351								
NGC 3521								
NGC 3627								
NGC 3773								
NGC 3938								
NGC 4125								
NGC 4254								
NGC 4321								
NGC 4536								
NGC 4552								
NGC 4569								
NGC 4579								
NGC 4725								
NGC 4736								
DDO 154								
NGC 4826								
DDO 165								
NGC 5194								
NGC 5398(Tol89)[b]								
NGC 5408[b]								
NGC 5713								
NGC 5866								
IC 4710								
NGC 6822								
NGC 7331								
NGC 7552								
NGC 7793								

[a]Fluxes and their (statistical) uncertainties are listed in units of 10^{-9} W m^{-2} sr^{-1}. Calibration uncertainties are an additional ~30%. The 6.2 μm PAH feature equivalent width is given in units of microns.

[b]The infrared emission peaks outside of the field of view of the spectral maps.

Table 2. Extranuclear Emission Line Fluxes and 6.2 μm PAH Feature Equivalent Widths [a]

Species	PAH	[SIV]	[NeII]	[NeIII]	[SIII]	[OIV]	[SIII]	[SiII]
Wavelength	6.2μm	10.51μm	12.81μm	15.56μm	18.71μm	25.89μm	33.48μm	34.82μm
Excitation (eV)		34.8	21.6	41.0	23.3	54.9	23.3	8.2
NGC 5194 CCM107								
NGC 5194 CCM072								
NGC 5194 CCM071								
NGC 5194 CCM001								
NGC 5194 CCM010								
NGC 5194 CCM071A								
NGC 3031 HK230								
NGC 3031 HK343								
NGC 3031 HK453								
NGC 3031 HK268								
NGC 3031 HK652								
NGC 3031 HK741								
NGC 3031 Munch1								
NGC 6946 H4								
NGC 6946 HK3								
NGC 6946 H288								
NGC 6946 H40								
NGC 6946 H28								
NGC 0628 H292								
NGC 0628 H572								
NGC 0628 H627								
NGC 0628 H013								
HolmbergII HSK45								
HolmbergII HSK67								
HolmbergII HSK70								
HolmbergII HSK07								

[a]Fluxes and their (statistical) uncertainties are listed in units of 10^{-9} W m^{-2} sr^{-1}. Calibration uncertainties are an additional $\sim$30%. The 6.2 μm PAH feature equivalent width is given in units of microns.

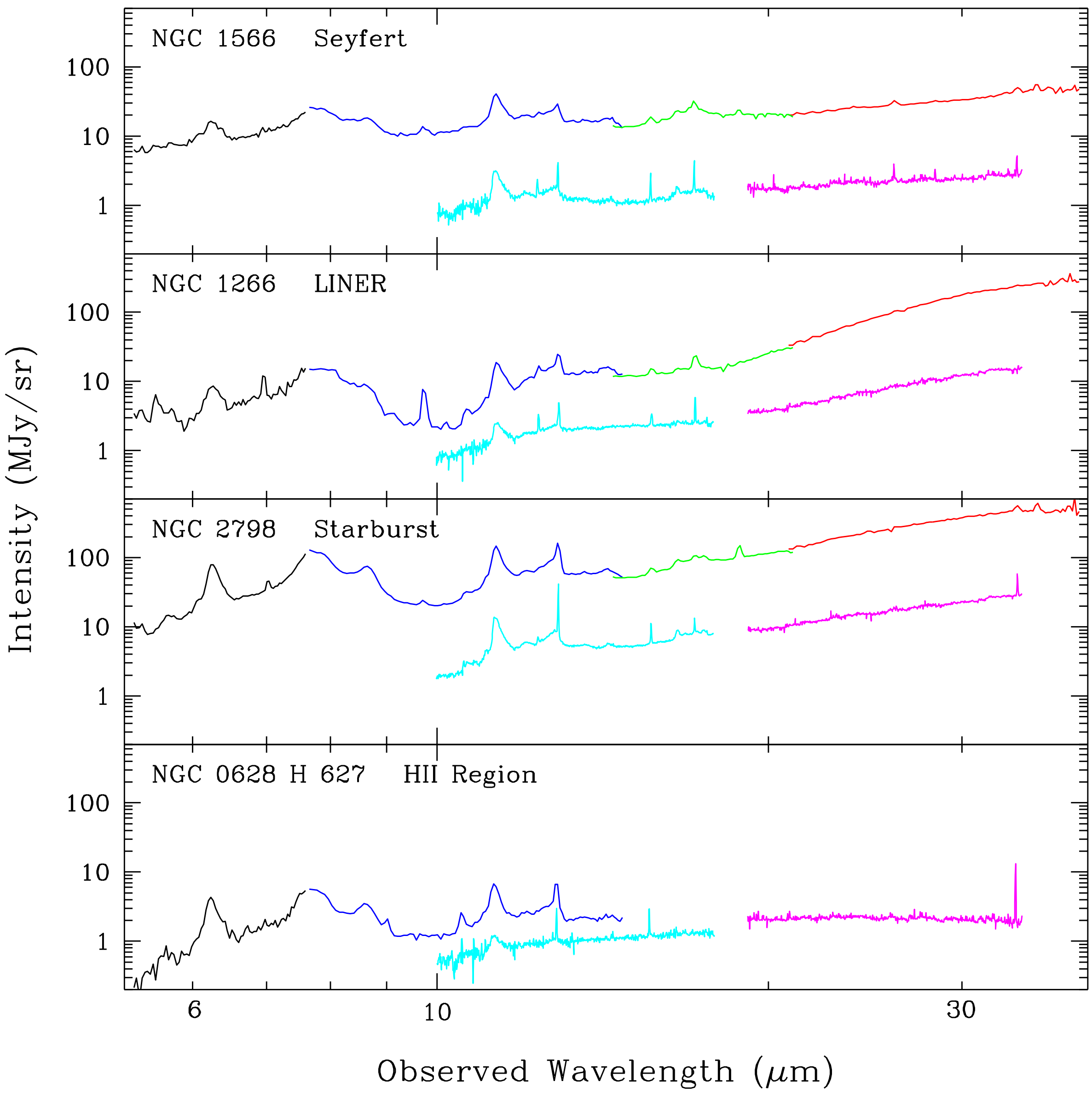

Fig. 1.— An example of both low- and high-resolution spectra for four different types of environments found within the SINGS sample. Each color corresponds to a different IRS module: black→SL2, blue→SL1, green→LL2, red→LL1, cyan→SH, and magenta→LH. Each spectral segment has been extracted from a $\sim 23'' \times 15''$ region. The low-resolution data are sky-subtracted, unlike the high-resolution data, which are scaled downwards by 1.2 dex for clarity.

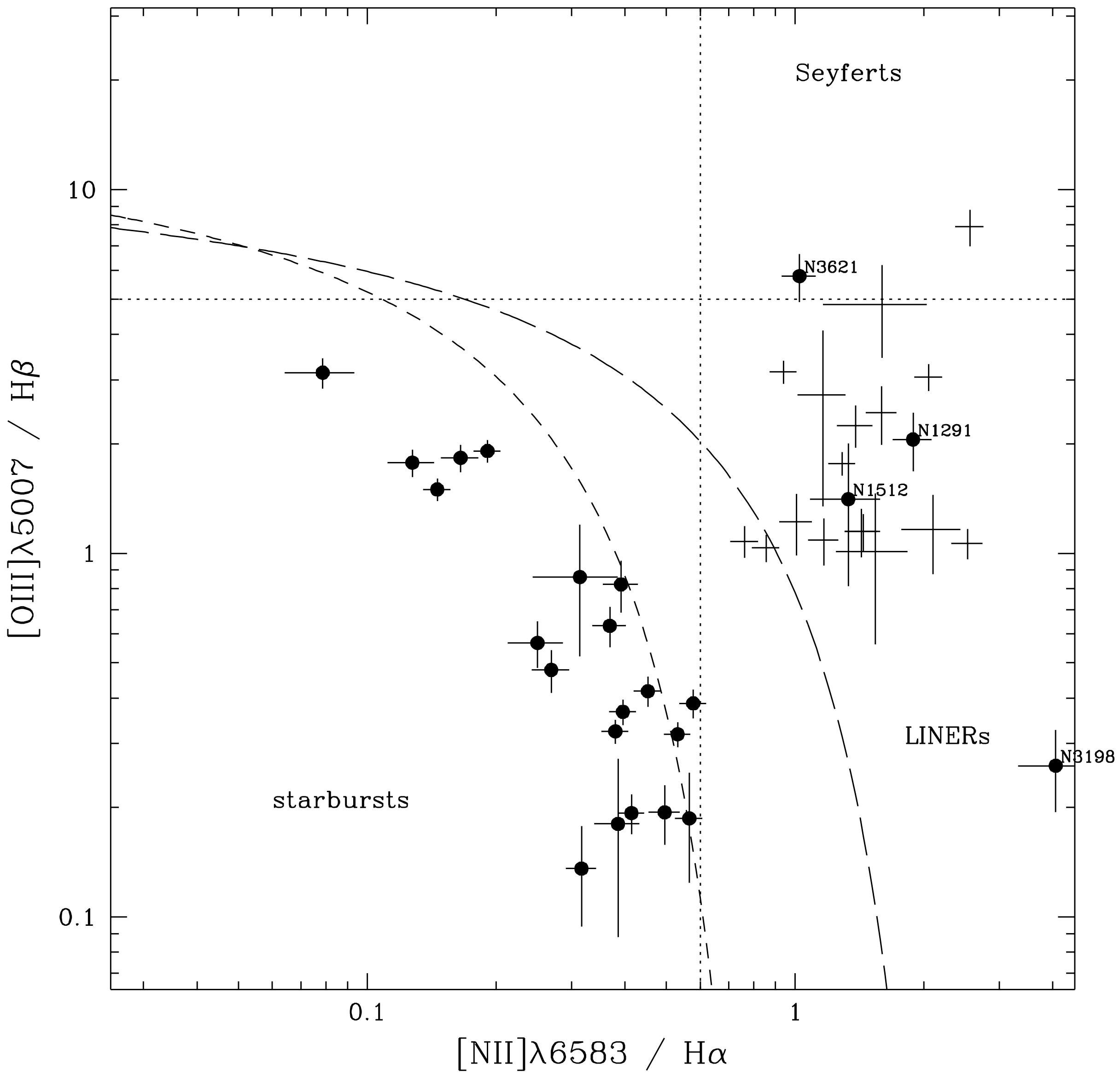

Fig. 2.— A traditional diagnostic diagram is displayed for the SINGS nuclei using optical data and 2.″5×2.″5 apertures. Filled circles mark galaxies for which NED does not indicate an active nucleus (LINER or Seyfert). The dotted lines delineate typical starburst/AGN/LINER boundaries: [O III]5007/Hβ $\sim$ 5 and [N II]6583/Hα $\sim$ 0.6 (e.g. Armus, Heckman, & Miley 1989). The long-dashed and short-dashed curves respectively trace the empirical starburst/AGN boundaries of Kewley et al. (2001) and Kauffmann et al. (2003).

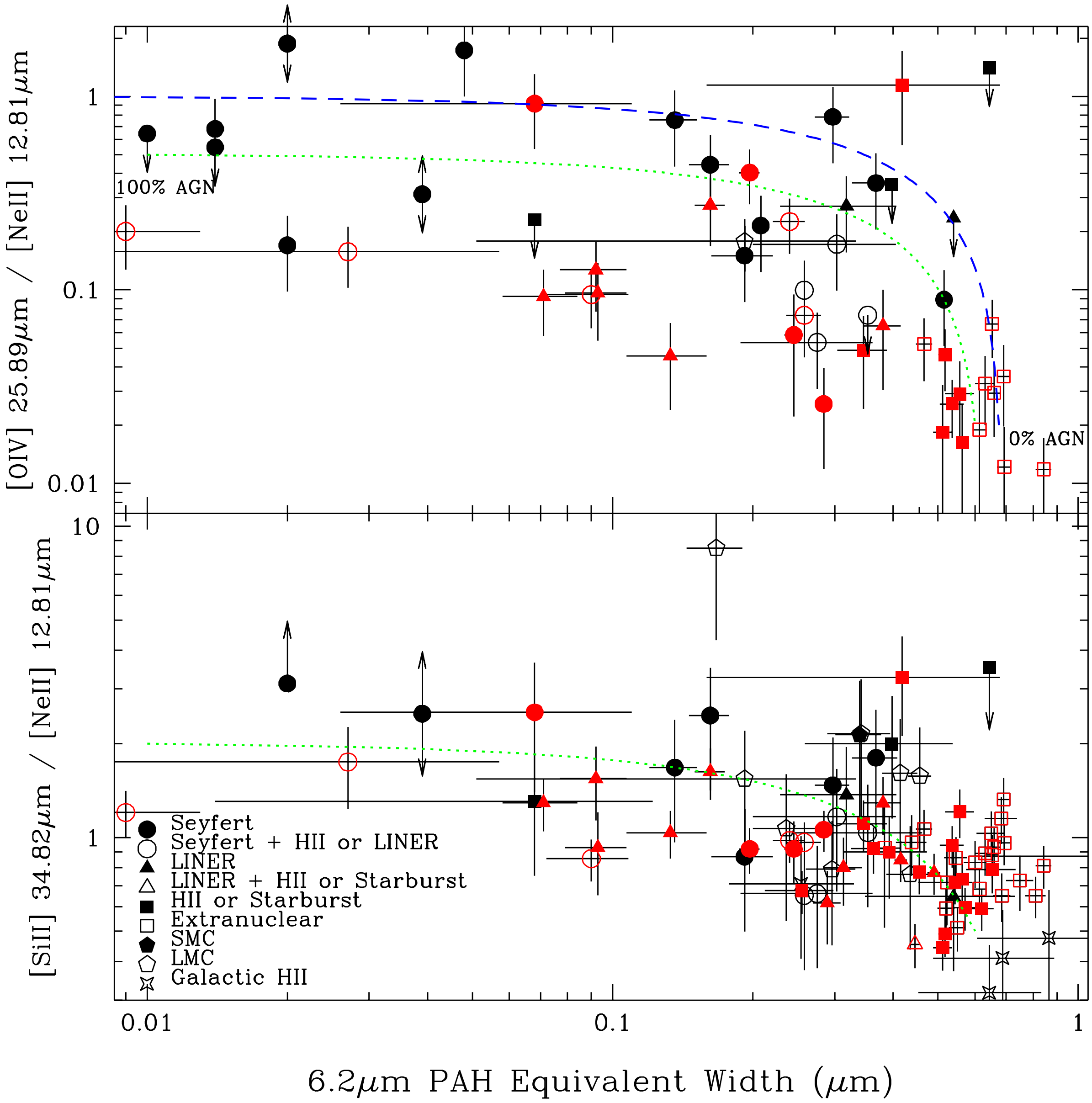

Fig. 3.— The ratios of mid-infrared forbidden lines as a function of the 6.2 μm PAH feature equivalent width. SINGS data are displayed in red; archival data are indicated with black symbols and described in § 3.2. The dotted lines are linear mixing models of a "pure" AGN and a "pure" star-forming source (see text). The dashed line is a similar mixing model first presented in Genzel et al. (1998).

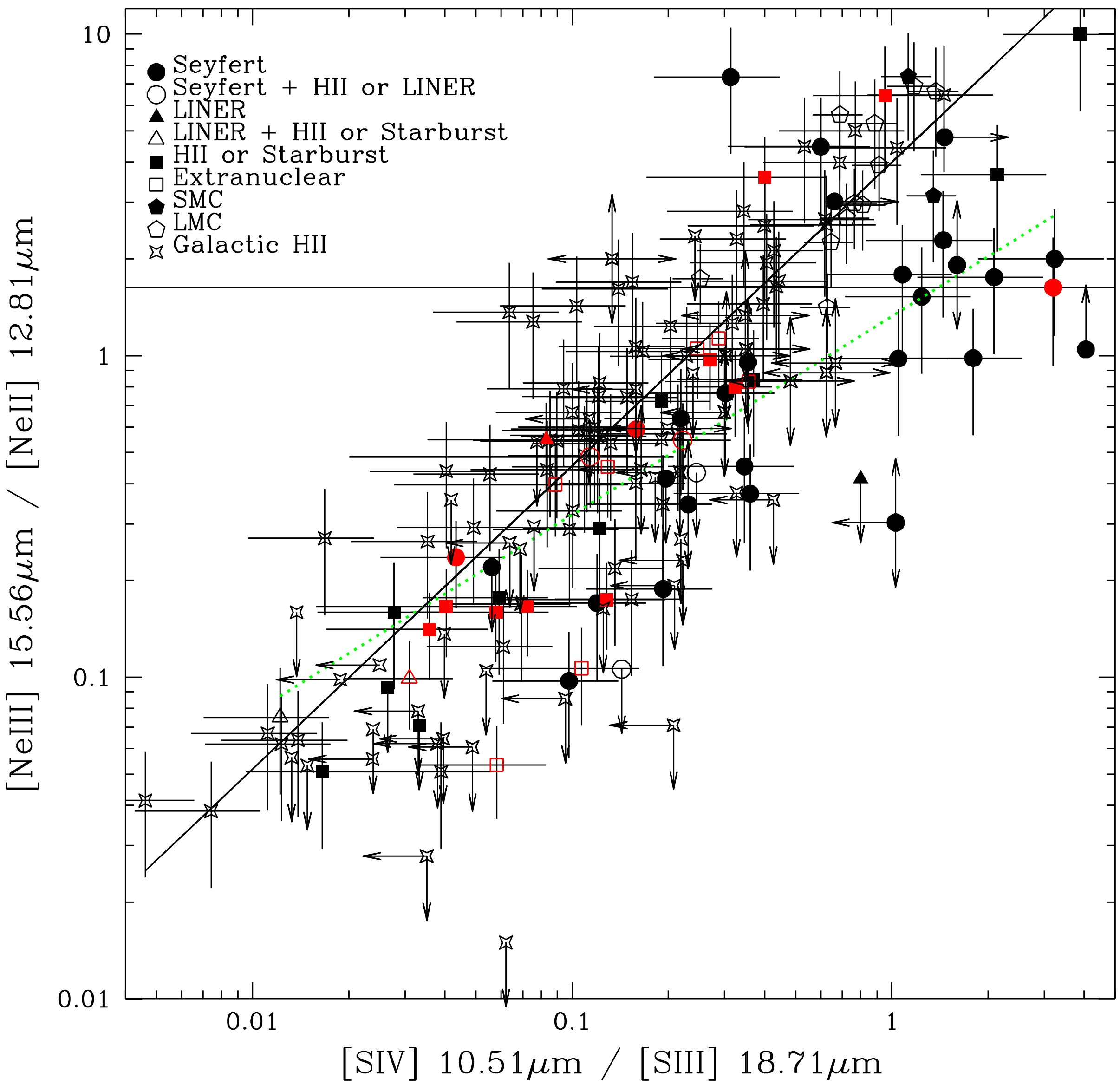

Fig. 4.— A diagnostic diagram involving ratios of Neon and Sulfur lines at different ionization levels is displayed. SINGS data are displayed in red; archival data are indicated with black symbols and described in § 3.2. The solid line is a linear fit to the detections of star-forming nuclei and H II regions, while the dotted line is linear fit to the AGN detections.

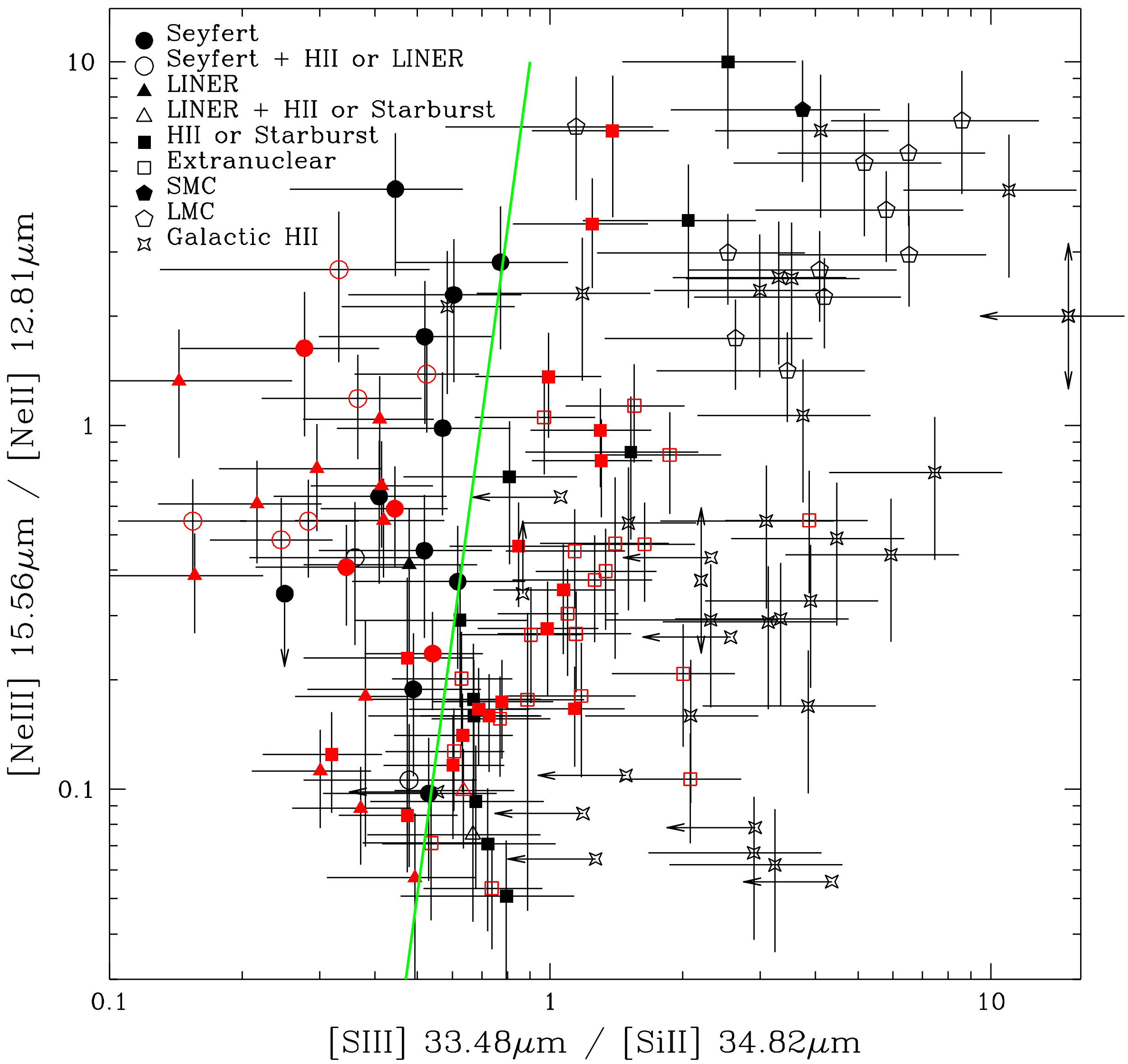

Fig. 5.— A Neon, Sulfur, and Silicon diagnostic diagram involving ratios of lines at different ionizations is displayed. SINGS data are displayed in red; archival data are indicated with black symbols and described in § 3.2. The dotted line delineates the approximate boundary between AGN and star-forming sources.

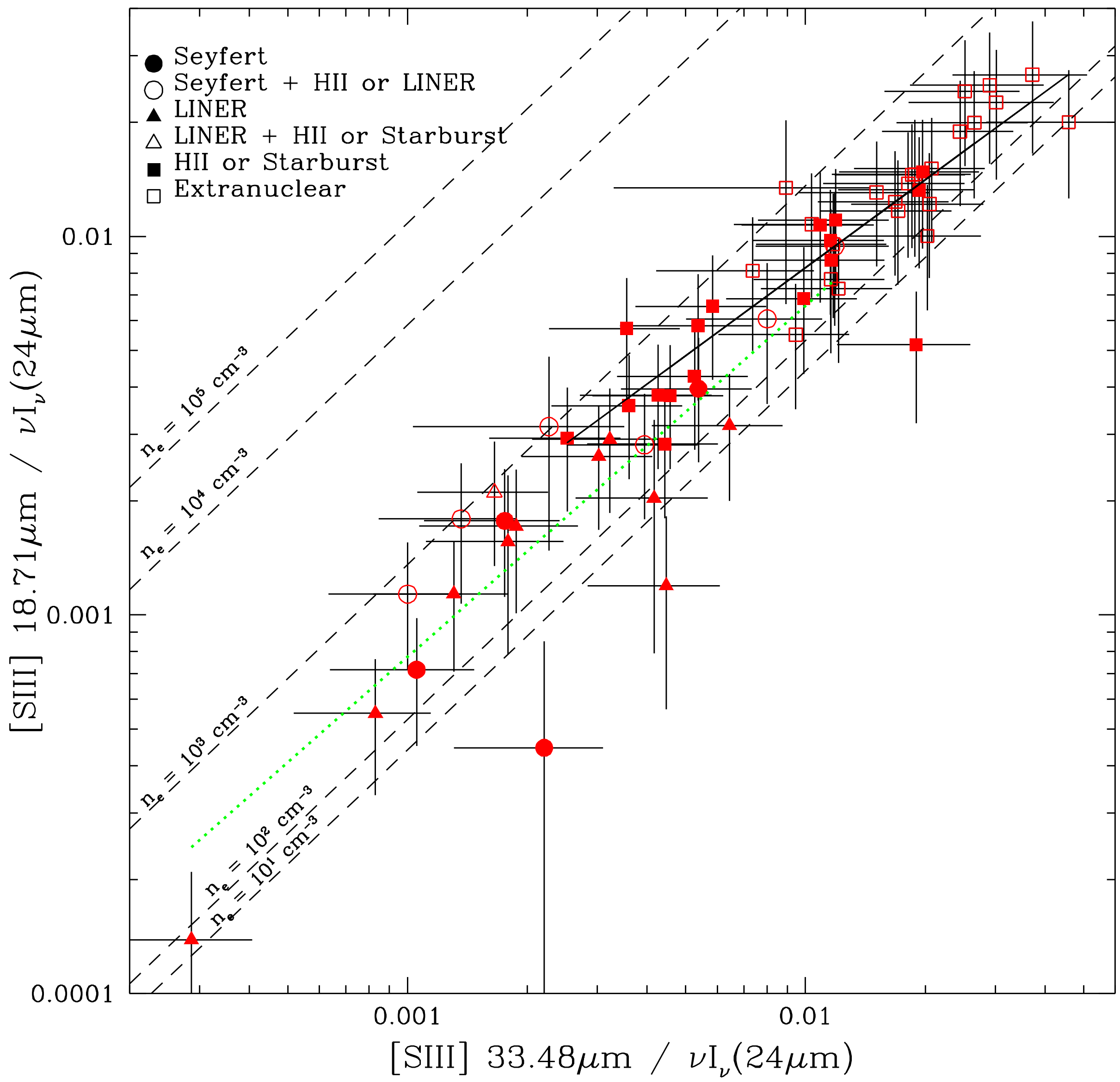

Fig. 6.— The correlation between two transitions of doubly-ionized Sulfur is displayed, normalized by the flux at 24 μm. This plot only includes SINGS data. The solid line is a linear fit to the detections of star-forming nuclei and H II regions, while the dotted line is linear fit to the AGN detections. The set of dashed lines represent different constant interstellar electron densities. The SINGS data typically exhibit $n_{\rm e} \sim 400$ cm^{-3}.